

Stable dynamic helix state in the nonintegrable XXZ Heisenberg model

G. Zhang and Z. Song[†]

E-mail: songtc@nankai.edu.cn

School of Physics, Nankai University, Tianjin 300071, China

Abstract. We investigate the influence of external fields on the stability of spin helix states in an XXZ Heisenberg model. Exact diagonalization on a finite system shows that random transverse fields in the x and y directions drive the transition from integrability to nonintegrability. In such a system, the helix state can be regarded as a quantum scar. Simultaneously, the presence of uniform z field enables the helix state to better maintain its dynamical nature, allowing for a clearer understanding of its evolutionary behavior. However, the entanglement entropy reveals that irrespective of the presence of a uniform z field, as long as the system remains chaotic, the scar extent of the helix state shows no significant variation.

PACS numbers: 05.45.Mt, 05.70.-a, 67.57.Lm, 03.67.-a

Keywords: Quantum Scar, Quantum Thermalization, Spin dynamics, Quantum information

1. Introduction

The thermalization of quantum systems is one of the main obstacles for quantum simulation and quantum information processing, because the process of thermalization always eventually destroys the information of an initial state. It is expected that there are exceptional cases where some special slowly thermalizing initial states retain the memory over longer periods of time. Specifically, it is well established that some nonintegrable systems can fail to thermalize due to rare nonthermal eigenstates called quantum many-body scars (QMBS) [1–19]. These nonthermal states are typically excited ones and span a subspace, in which any initial states do not thermalize and can return periodically. The main task in this field is finding scars in a variety of nonintegrable many-body systems. On the other hand, a modern challenge in condensed matter physics is searching for long-lived non-thermal excited states that possess macroscopic long-range order. In contrast to the ground state, which is based on a cooling down mechanism, the preparation of such states can be obtained via dynamic process.

Atomic systems are an excellent test-beds for quantum simulator in experiments [20–26], stimulating theoretical studies on the dynamics of quantum spin systems. These studies not only capture the properties of many artificial systems, but also provide tractable theoretical examples for understanding fundamental concepts in physics. As a paradigmatic quantum spin model, the Heisenberg XXZ model exhibits strong correlations and its dynamical properties attract attention from both the condensed matter physics and mathematical-physics communities [27–30]. Furthermore, recent experimental advances in cold-atom systems enable realizations of the XXZ chain and preparation of certain initial states [31, 32], providing an ideal platform for studying nonequilibrium quantum dynamics. Specifically, the discovery of highly excited many-body eigenstates of the XXZ Heisenberg model, referred to as Bethe phantom states, has received much attention from both theoretical [33–36] and experimental approaches [32, 37–39]. Previous work has examined the issue of many-body localization (MBL) arising from strong disorder in a generalized XXZ model [40]. Here, our primary focus is on investigating whether the helix state can become a quantum scar in the XXZ model in the absence of MBL. Although the XXZ chain is an integrable system, the helix states are not supported by the symmetry of the model [36]. Therefore, they are regarded as a candidate of quantum scars in the presence of perturbation. Importantly, a helix state essentially supports macroscopic long-range order in an ultracold atom quantum simulator [39]. However, it is still an open question what happens if the XXZ chain becomes nonintegrable in the presence of random field.

In this work, we investigate the influence of the external fields on the stability of spin helix states in an XXZ Heisenberg model. We consider two types of fields, (i) uniform field in z direction; (ii) random transverse fields in x and y directions. These two fields are shown to play different roles on the dynamics of a static helix state, which is the eigenstate of an unperturbed XXZ Heisenberg model. Exact diagonalization on

a finite system shows that random transverse fields in x and y directions drive the transition from integrability to nonintegrability. The energy level statistics is a Poisson distribution for weak random field, but becomes Wigner–Dyson from Gaussian Unitary Ensemble (WD-GUE) distribution as the strength of the random field increases. In the absence of the uniform z field, the random field causes the deviation of the evolved state from the original helix state. However, in the presence of uniform z field, the static helix state becomes a dynamic helix state with a relatively long life as a quantum scar state. We analyze the underlying mechanism in the framework of perturbation method. It manifests that the uniform field can suppress the effect of the random field. Numerical simulations for the dynamics of a helix state show that (i) in the presence of uniform field, a helix state exhibits a near perfect revival as quantum scars; (ii) in the absence of uniform field, although the helix state deviates from being an eigenstate, it still maintains a profile of a helix state within a long time.

The rest of this paper is organized as follows: In Sec. 2, we introduce the model Hamiltonian and the helix states arising from towers. With these preparations, in Sec. 3 we present two types of helix states arising from towers. We demonstrate the phase diagram of the system in Sec. 4 by means of statistics of energy levels. Sec. 5 contributes to the dynamics of the helix states in the nonintegrable system. Sec. 6 concludes this paper.

2. Model Hamiltonian and precise towers

We begin this section by introducing a Hamiltonian

$$H = H_0 + H_{\text{ran}} \quad (1)$$

which consists of two parts. The unperturbed system

$$H_0 = \sum_{j=1}^N [s_j^x s_{j+1}^x + s_j^y s_{j+1}^y + \cos q (s_j^z s_{j+1}^z - \frac{1}{4}) + h s_j^z]$$

describes quantum spin XXZ Heisenberg chain with resonant anisotropy via wave vector $q = 2\pi n/N$ ($n \in [0, N-1]$), in a uniform field in the z direction, and the perturbation term

$$H_{\text{ran}} = \sum_j (x_j s_j^x + y_j s_j^y), \quad (2)$$

is the subjected random fields along the x and y -direction. Here the field distribution is $x_j = \text{ran}(-x, x)$ and $y_j = \text{ran}(-y, y)$, where $\text{ran}(-b, b)$ denotes a uniform random number within $(-b, b)$. Here s_j^λ ($\lambda = x, y, z$) are canonical spin-1/2 variables, and obey the periodic boundary condition $s_{N+1}^\lambda \equiv s_1^\lambda$.

We start with the case where $x = y = 0$, which serves as the basis for the rest of the study. We introduce a set of q -dependent spin operators

$$s_q^+ = (s_q^-)^\dagger = \sum_{j=1}^N e^{iqj} s_j^+, \quad s^z = \sum_{j=1}^N s_j^z,$$

which not surprisingly satisfy the Lie algebra commutation relations

$$[s_q^+, s_q^-] = 2s^z, [s^z, s_q^\pm] = \pm s_q^\pm. \quad (3)$$

Unlike the isotropic case with $q = 0$, H_0 does not have $SU(2)$ symmetry. However, when we consider a subspace W spanned by a set of states $\{|\psi_n\rangle\}$ ($n \in [0, N]$), which is defined as

$$|\psi_n\rangle = \frac{1}{\Omega_n} (s_q^+)^n |\Downarrow\rangle. \quad (4)$$

Here the normalization factor $\Omega_n = (n!) \sqrt{C_N^n}$, and then we have $|\psi_0\rangle = |\Downarrow\rangle = \prod_{j=1}^N |\Downarrow\rangle_j$ and $|\psi_N\rangle = e^{iq(1+N)N/2} |\Uparrow\rangle$, with $|\Uparrow\rangle = \prod_{j=1}^N |\Uparrow\rangle_j$, with $s_j^z |\Downarrow\rangle_j = -1/2 |\Downarrow\rangle_j$ ($s_j^z |\Uparrow\rangle_j = 1/2 |\Uparrow\rangle_j$). Importantly, straightforward derivation shows that $\{|\psi_n\rangle\}$ is a set of eigenstates of H_0 , i.e.,

$$H_0 |\psi_n\rangle = (n - N/2) h |\psi_n\rangle. \quad (5)$$

Remarkably, it ensures that

$$\{[H_0, s_q^\pm] \mp h s_q^\pm\} W = 0, \quad (6)$$

which indicates that $\{|\psi_n\rangle\}$ is a precise tower of energy according to the theorem in Ref. [41]. In parallel, state

$$|\bar{\psi}_n\rangle = \frac{1}{\Omega_n} (s_{-q}^+)^n |\Downarrow\rangle, \quad (7)$$

is also eigenstates of H_0 , which share the same energy with $|\psi_n\rangle$. Studies have shown that quantum scars can be generated through towers [19, 42, 43]. Additionally, research indicates that introducing perturbations into the Heisenberg model can transition the system from integrable to chaotic, while the towers persist [44]. Inspired by this, if after introducing perturbations, this model can also become chaotic and the towers survive, the towers will be able to generate quantum scars. We will discuss this in detail in Secs. 4 and 5.

3. Static and dynamic helix states

In this section, we will introduce two types of helix states based on the eigenstates of H_0 . A generalized helix state is defined by a state in the form

$$|\Phi\rangle = \prod_{j=1}^N \left[\cos(\theta/2) |\Uparrow\rangle_j + e^{i\Lambda(j,t)} \sin(\theta/2) |\Downarrow\rangle_j \right], \quad (8)$$

which is obviously an unentangled state. It represents the tensor product of all spin precession states, forming a standard helix state. This is a physically interesting state that has recently been studied both theoretically and experimentally [33–36, 39]. So far, the study of this state mainly focuses on a simple case with $\Lambda(j, t) = qj + \omega t$. State $|\Phi\rangle$ with zero ω is the eigenstate of a fine-tuned XXZ Heisenberg ring with zero external field. Here θ is an arbitrary parameter, resulting in a set of degenerate states of the system. It

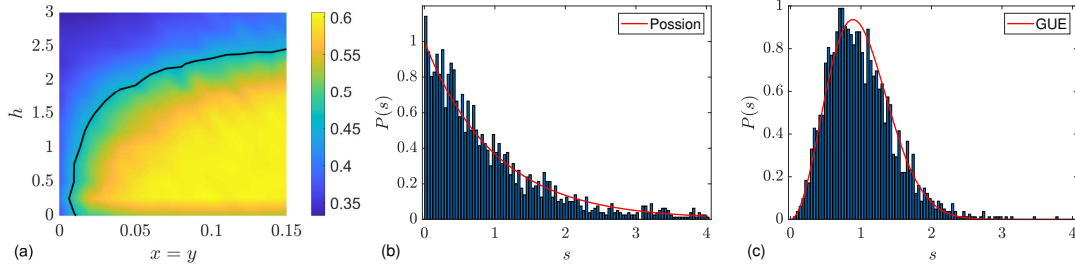


Figure 1. Exact diagonalization results on r -values and statistics of energy level spacings for the model on an $N = 12$ chain in Eq. (1) with representative parameters. The results are obtained from the average over 10 sets of random number. (a) Color contour plot of the average level spacing ratio r as a function of h and x . There are two regions separated by the black contour line. The distribution of $r(h, x)$ indicates the phase diagram: The blue region represents the integrable phase and the yellow region represents the nonintegrable phase. (b, c) Plots of $P(s)$ for two typical cases: $x = y = 0.0$ and $x = y = 0.05$, respectively. In both cases, the field $h = 0.5$. In order to avoid the unexpected degeneracy, the coupling strength for the term $s_1^x s_N^x$ is taken as 0.85. The red lines indicate Poisson and WD-GUE distributions for comparison, the characteristic of integrable and chaotic systems described by random matrix theory. As expected, the distributions agree with the phase diagram in (a).

allows a multiple occupation of a single magnon mode with nonzero wave vector q , as an analog of a Goldstone mode in the anisotropic Heisenberg model [36]. In this work, we focus on the case with nonzero ω , arising from nonzero external field. We introduce a local vector $\mathbf{h}_l = (h_l^x, h_l^y, h_l^z)$ with $h_l^\alpha = \langle \psi | s_l^\alpha | \psi \rangle$ ($\alpha = x, y, z$) to characterize the helicity of a given state $|\psi\rangle$. For eigenstates $|\psi_n\rangle$, straightforward derivation of $h_l^\alpha(n) = \langle \psi_n | s_l^\alpha | \psi_n \rangle$ show that

$$h_l^x(n) = h_l^y(n) = 0, h_l^z(n) = \frac{n}{N} - \frac{1}{2},$$

which is uniform, indicating that $|\psi_n\rangle$ is not a helix state. Nevertheless, in the following we will show that their superposition can be helix states. These states can be classified into two types of helix states: static and dynamic helix states.

3.1. Static helix states

We consider a superposition eigenstates in the form

$$|\phi(\theta)\rangle = \sum_n d_n |\psi_n\rangle, \quad (9)$$

where

$$d_n = \sqrt{C_N^n} (-i)^n \sin^n(\theta/2) \cos^{(N-n)}(\theta/2). \quad (10)$$

The corresponding helix vector is

$$\mathbf{h}_l = \frac{1}{2} [\sin \theta \sin(ql), \sin \theta \cos(ql), -\cos \theta], \quad (11)$$

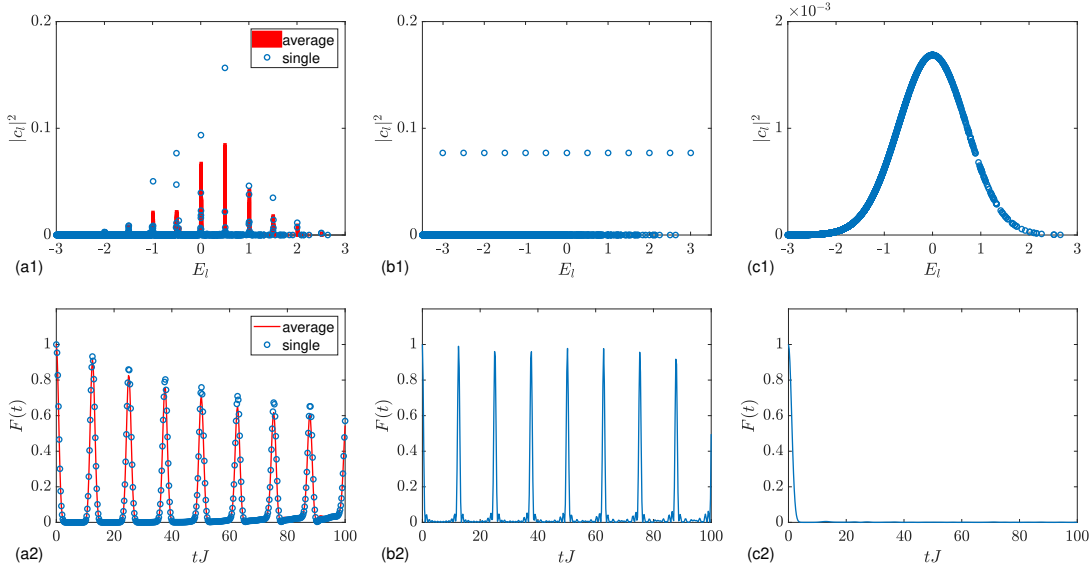


Figure 2. Plots of the fidelity from Eq. (23) for three typical initial states. The parameters are $N = 12$, $x = y = 0.05$ and $h = 0.5$. The top panel displays the distribution of expansion coefficients $|c_l|^2$ across energy level. The bottom panel displays the fidelity. (a1), (a2) For the helix state. The red bar and red line are obtained from the average over 20 sets of random numbers. (b1), (b2) For a linear superposition of quantum states $|\varphi_l\rangle$, which has the maximum overlap with quantum state $|\psi_n\rangle$. (c1), (c2) For an initial state with a Gaussian distribution. We find that the helix state exhibits periodic revival phenomena, whereas the Gaussian state does not.

which indicates that $|\phi(\theta)\rangle$ is a helix state for nonzero $\sin \theta$. Here θ is an arbitrary angle and determines the profile of the state. This can be obtained easy when we express it in the form.

$$|\phi(\theta)\rangle = \prod_{j=1}^N [\cos(\theta/2) |\downarrow\rangle_j - ie^{iqj} \sin(\theta/2) |\uparrow\rangle_j]. \quad (12)$$

It represents a tensor product of the precession states of all spins, which is an unentangled state. It accords with the result $|\mathbf{h}_l|^2 = 1/4$. The state $|\phi(\theta)\rangle$ is referred to as a static helix state since it is time-independent. In parallel state

$$|\bar{\phi}(\theta)\rangle = \prod_{j=1}^N [\cos(\theta/2) |\downarrow\rangle_j - ie^{-iqj} \sin(\theta/2) |\uparrow\rangle_j], \quad (13)$$

is another one with opposite helicity. We note that both $|\phi(\theta)\rangle$ and $|\bar{\phi}(\theta)\rangle$ are also eigenstates of H_0 with zero h . Some studies have already explored the dynamic generation of helix states driven by local non-Hermitian fields in the XXZ Heisenberg model with the Dzyaloshinskii-Moriya interaction [45, 46], and now we are investigating how these helix states evolve when an external field is applied.

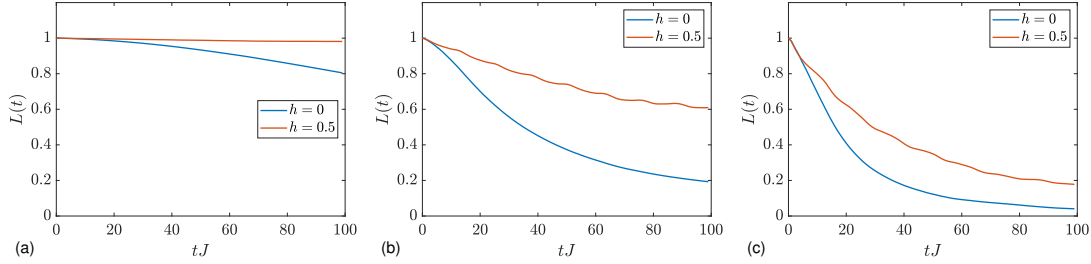


Figure 3. Plots of the Loschmidt echo from (24) at different disorder strength, where $N = 12$, $h = 0, 0.5$. (a) For $x = y = 0.01$. (b) For $x = y = 0.05$. (c) For $x = y = 0.1$. We find that the increase in disorder strength will intensify the decay of the Loschmidt echo, while increasing the magnetic field strength will suppress the decay of the Loschmidt echo.

3.2. Dynamic helix states

When the external field h switches on, $|\phi(\theta)\rangle$ and $|\bar{\phi}(\theta)\rangle$ are no longer the eigenstates of H_0 . Considering $|\phi(\theta)\rangle$ as initial state at $t = 0$, the evolved state is

$$\begin{aligned} |\phi_0(\theta, t)\rangle &= e^{-iE_0 t} \sum_n e^{-inh t} d_n |\psi_n\rangle \\ &= e^{-iE_0 t} \times \prod_{j=1}^N [\cos(\theta/2) |\downarrow\rangle_j - i e^{i(qj - ht)} \sin(\theta/2) |\uparrow\rangle_j], \end{aligned} \quad (14)$$

where $E_0 = -Nh/2$. The corresponding helix vector is

$$\mathbf{h}_l = \frac{1}{2} [\sin \theta \sin (ql - ht), \sin \theta \cos (ql - ht), -\cos \theta], \quad (15)$$

which satisfies the travelling-wave relation

$$\mathbf{h}_l(t) = \mathbf{h}_{l - ht/q}(0). \quad (16)$$

This indicates that $|\psi(t)\rangle$ acts as a travelling wave with phase velocity h/q , then is referred to as dynamic helix state. Obviously, it is also a perfect periodic function of time, and then the system exhibits a perfect revival. To demonstrate this phenomenon, plots of h_l for several typical cases are presented in Fig. 4.

4. Level statistics

A popular approach to distinguishing between integrable and nonintegrable model involves studying spectral statistics using tools derived from random matrix theory. For a nonintegrable model, the statistical distribution of level spacings follows the Wigner-Dyson distribution, while integrable models follow the Poisson distribution. This distribution can also be directly detected using the average level spacing ratio r -value [47, 48], which is the average of

$$r_l = \frac{\min\{s_l, s_{l+1}\}}{\max\{s_l, s_{l+1}\}}, \quad (17)$$

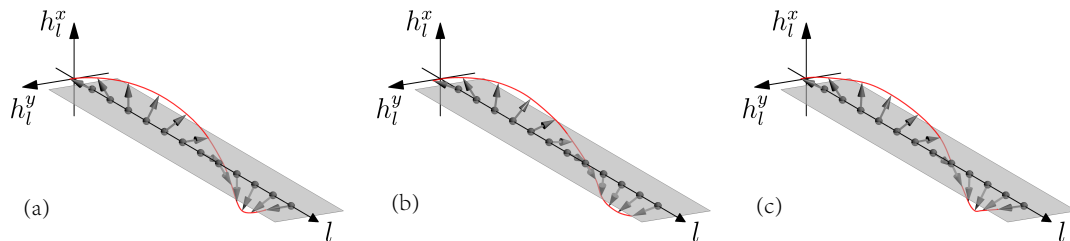


Figure 4. Plots of the profile of the time evolution for the helix state in Eq. (12) with $\theta = \pi/2$ as the initial state under the Hamiltonian H with $x = y = 0.05$ and $h = 0$. (a) For $tJ = 0$. (b) For $tJ = 20$. (c) For $tJ = 100$. The corresponding Loschmidt echo $L(t)$ is plotted Fig. 3(b). It indicates that evolved states are apparently still helix states with a slight deformation although the fidelity becomes lower. The explanation is given in the text.

where s_l is level spacings $E_l - E_{l-1}$ for a selected set of energy levels $\{E_l\}$. $r \approx 0.53$ and $r \approx 0.60$ for Wigner–Dyson from Gaussian Orthogonal Ensemble (WD-GOE) and WD-GUE distributions, respectively, and $r \approx 0.39$ for the Poisson distribution. This has been used in several works [18, 40, 44, 49, 50]. The XXZ Heisenberg model is known to be integrable by Bethe ansatz methods [51]. However, in the presence of H_{ran} , we will show the integrability of the system is destroyed based on numerical results for a finite-size system. In Fig. 1, we depict a phase diagram illustrating the average level spacing ratio r plotted against h vs disorder strength in the x plane. As evident from the figure, a transition from integrable to nonintegrable phases is observed.

On the other hand, we also computed the statistical distribution of the spacings s between energy levels, denoted as $P(s)$. We start with the case $x = y = 0$, but arbitrary h . The distribution $P(s)$ in each sector indexed by the spin component in z direction is anticipated to follow a Poisson distribution. Nevertheless, results obtained from exact diagonalization of a small-sized system reveal that a near-perfect Poisson distribution can be achieved when the translational symmetry is broken by a slight deviation in the coupling strength of a single dimer. In the scenario where x and y are nonzero, states in different sectors become hybridized, necessitating the calculation of $P(s)$ across all levels. In Fig. 1, we illustrate the level spacing statistics of the model with a finite N . We take $x = y$ for simplicity, but with different random number series $\{x_j\}$ and $\{y_j\}$. We find that the level spacing distribution depends on the parameters (x, h) : (i) $(x, h) = (0, 0.5)$, $P(s)$ follows the Poisson distribution as expected; (ii) $(x, h) = (0.05, 0.5)$, $P(s)$ follows the WD-GUE distribution.

5. Quantum scars and stable helix states

As excited states, the energy levels for the subspace $\{|\psi_n\rangle\}$ and the helix state merge into the dense spectrum. It has been proposed that the subspace $\{|\psi_n\rangle\}$ is not supported by a symmetry of the Hamiltonian H_0 [36]. Therefore, as long as the tower survive in the

presence of H_{ran} , even if it becomes a quasi-tower, it is a candidate for quantum scar of the perturbed Hamiltonian H . In this section, we focus on two questions by analytical analysis approximately and numerical simulations: (i) Is a helix state immune to the thermalization in the presence of H_{ran} ? (ii) Is the $\{|\psi_n\rangle\}$ really a quantum scar? In the following, we will demonstrate that the external field h can enhance the stability of helix states, while $\{|\psi_n\rangle\}$ can be a quantum scar even with the zero h field.

We start with the estimation of the effect of the random field in x direction on the dynamics of a helix state by considering a simplified perturbation field

$$H_{\text{ran}} = x_0 s_l^x, \quad (18)$$

which is a local field in x direction at site l . The matrix representation of Hamiltonian H in the subspace $\{|\psi_n\rangle\}$ is an $(N+1) \times (N+1)$ matrix M with nonzero matrix elements

$$(M)_{n,n+1} = (M)_{n+1,n}^* = e^{iql} \frac{x_0}{2N} \sqrt{n(N+1-n)}, \quad (19)$$

with $n = [1, N]$, and

$$(M)_{n,n} = (n-1-N/2)h, \quad (20)$$

with $n = [1, N+1]$. It is obviously solvable matrix with equal spacing energy levels, i.e.

$$E_n = (n-1-N/2) \sqrt{h^2 + \left(\frac{x_0}{N}\right)^2}, \quad (21)$$

with $n = [1, N+1]$. In the case with zero h , we have $E_n \approx \frac{x_0}{N}(n-1-N/2)$, while $E_n \approx (n-1-N/2)h$ in the case with $h^2 \gg (x_0/N)^2$. From the perspective of energy correction, the effect of H_{ran} becomes weak in the presence of field h . This implies that H_{ran} may damage the helix state even worse in the zero h field. It suggest that one can suppress the thermalization on the subspace $\{|\psi_n\rangle\}$ by h field.

Now we demonstrate and verify our prediction by numerical simulation on the dynamic processes. Our major aspects of concerns are (i) the revival of the helix state in comparison with a non-scarring state; (ii) the deviation of the evolved state in the presence of random field. Firstly, we consider the time evolutions for three types of initial states, which are expressed in the form

$$|\psi(0)\rangle = \sum_l c_l |\varphi_l\rangle \quad (22)$$

where $|\varphi_l\rangle$ is the eigenstate with energy E_l of the perturbed Hamiltonian H , i.e., $H|\varphi_l\rangle = E_l|\varphi_l\rangle$. Here $\{E_l, |\varphi_l\rangle\}$ depends on the generated random number series. Three types of $\{c_l\}$ are obtained from 1) $|\psi(0)\rangle = |\phi(\pi/2)\rangle$; 2) Let the quantum state $|\psi(0)\rangle$ be a linear superposition of quantum states $|\varphi_l\rangle$, which has the maximum overlap with the quantum state $|\psi_n\rangle$; 3) Gaussian distribution of $\{c_l\}$. We introduce the quantity

$$F(t) = |\langle\psi(t)|\psi(0)\rangle|^2 \quad (23)$$

to characterize the quality of the revival. The plots of $F(t)$ in Fig. 2 for several typical cases show that the revival strongly depends on the initial state. The time evolution in 2(b1, b2) shows that the near perfect revival can be achieved even in the nonintegrable

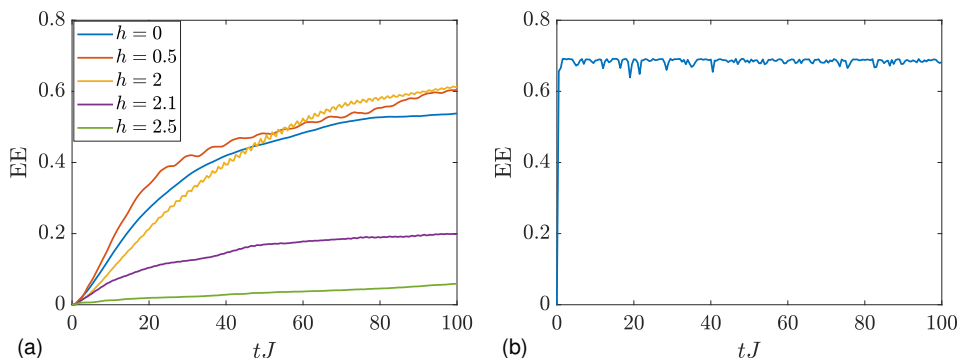


Figure 5. Plots of the entanglement entropy for helix state and Neel state, where $N = 12$, $x = y = 0.05$. (a) For the helix state with $h = 0, 0.5, 2, 2.1, 2.5$. (b) For the Neel state with $h = 0.5$. All of them are obtained from the average over 20 sets of random number. We find that when h is less than 2, the influence on the entanglement entropy of the helix state is minimal. However, when h exceeds 2, the entanglement entropy is rapidly suppressed. In either scenario, the growth of entanglement entropy of the helix state is significantly slower than that of the Neel state.

system. It indicates that the tower remains stable after the introduction of perturbation, and this long-lived oscillatory dynamics of the helix state can serve as evidence for helix state being a quantum scar. Secondly, we measure the influence of random and uniform field on the helix state and explore methods to enhance the stability of the helix state under perturbations. We consider the time evolutions of a same state under two driven Hamiltonian. In this case, the Loschmidt echo defined by

$$L(t) = |\langle \phi(\theta, t) | \phi_0(\theta, t) \rangle|^2 \quad (24)$$

is usually employed, with $|\phi(\theta, t)\rangle = e^{-iHt} |\phi(\theta)\rangle$ and $|\phi_0(\theta, t)\rangle = e^{-iH_0 t} |\phi(\theta)\rangle$. In Fig. 3, we plot the Loschmidt echo obtained from systems with different disorder strength and uniform field h . Because $|\phi_0(\theta, t)\rangle$ can maintain a perfect helix state, the Loschmidt echo can reflect the extent to which the dynamic behavior deviates from the helix state under perturbations. It is evident that the decay of Loschmidt echo accelerates with increasing disorder strength. This is easily understood, but it is worth noting that regardless of the level of disorder strength, introducing a uniform magnetic field consistently suppresses the decay of Loschmidt echo. This indicates that the uniform magnetic field can enhance the stability of the helix state.

However, we would like to point out that the fast decay of Loschmidt echo does not indicate the collapse of the helix state, but may be only different from the state $|\phi_0(\theta, t)\rangle$. We demonstrate this point by the plots of \mathbf{h}_i for $|\phi(\theta, t)\rangle$ in Fig. 4. We compute the time evolution for extreme case, in which the Loschmidt echo decays must faster. Numerical results show that the profile of the helix state changes slightly. This can be explained by the estimation on the Loschmidt echo of individual spin when $L(t) = 0.2$ and 0.6 , for example, $\sqrt[12]{0.2} = 0.87$, $\sqrt[12]{0.6} = 0.96$, which is similar to the orthogonality catastrophe by Anderson [52, 53].

Based on this, a favorable result of Loschmidt echo can indicate that the scar behavior is indeed favorable and help people know how the scar evolves in experiment, but a decay of Loschmidt echo does not necessarily imply poor scar behavior. Therefore, we also investigated the entanglement entropy (EE) of the helix state to measure its scar extent. The entanglement entropy is defined as $-\text{Tr}(\rho_A \log \rho_A)$, where A is the reduced density matrix of the subsystem A. Due to symmetry considerations, we select the first spin as the subsystem in this context. The results of the entanglement entropy under various uniform fields h are depicted in Fig. 5(a). It can be observed that when the uniform field h is less than 2, it has minimal impact on the entanglement entropy. However, when h exceeds 2, the entanglement entropy rapidly suppressed. This phenomenon is attributed to the system transitioning from chaotic to integrable, as illustrated in Fig. 1(a). Since the entanglement entropy of the Gaussian state is inherently high, which is unfavorable for observing the evolution results, we plotted the entanglement entropy of the Neel state, a commonly used quantum state in quantum information, in Fig. 5(b). By comparison, it is evident that as long as the system remains chaotic, regardless of the value of h , the helix state can be considered a robust quantum scar.

6. Conclusion

In summary, we have investigated the influence of the external fields on the stability of spin helix states in a XXZ Heisenberg model. Exact diagonalization on a finite system shows that random transverse fields in x and y directions drive the transition from integrability to nonintegrability. In such a system, the helix state can be regarded as quantum scar. Simultaneously, the presence of uniform z field enables the helix state to better maintain its dynamical nature, allowing for a clearer understanding of its evolution behavior. However, the entanglement entropy reveals that irrespective of the presence of uniform z field, as long as the system remains chaotic, the scar extent of the helix state shows no significant variation. It is expected to be insightful for quantum engineering of a helix state in experiments.

Acknowledgments

We acknowledge the support of the National Natural Science Foundation of China (Grants No. 11705127 and No. 11874225).

References

- [1] Shiraishi N and Mori T 2017 Systematic Construction of Counterexamples to the Eigenstate Thermalization Hypothesis *Phys. Rev. Lett.* **119** 030601
- [2] Moudgalya S, Rachel S, Bernevig B A and Regnault N 2018 Exact excited states of nonintegrable models *Phys. Rev. B* **98** 235155

- [3] Moudgalya S, Regnault N and Bernevig B A 2018 Entanglement of exact excited states of Affleck-Kennedy-Lieb-Tasaki models: Exact results, many-body scars, and violation of the strong eigenstate thermalization hypothesis *Phys. Rev. B* **98** 235156
- [4] Khemani V, Laumann C R and Chandran A 2019 Signatures of integrability in the dynamics of Rydberg-blockaded chains *Phys. Rev. B* **99** 161101(R)
- [5] Ho W W, Choi S, Pichler H and Lukin M D 2019 Periodic Orbits, Entanglement, and Quantum Many-Body Scars in Constrained Models: Matrix Product State Approach *Phys. Rev. Lett.* **122**, 040603
- [6] Shibata N, Yoshioka N and Katsura H 2020 Onsager's Scars in Disordered Spin Chains *Phys. Rev. Lett.* **124** 180604
- [7] McClarty P A, Haque M, Sen A and Richter J 2020 Disorder-free localization and many-body quantum scars from magnetic frustration *Phys. Rev. B* **102** 224303
- [8] Richter J and Pal A 2022 Anomalous hydrodynamics in a class of scarred frustration-free Hamiltonians *Phys. Rev. Research* **4** L012003
- [9] Jeyaretnam J, Richter J and Pal A 2021 Quantum scars and bulk coherence in a symmetry-protected topological phase *Phys. Rev. B* **104** 014424
- [10] Turner C J, Michailidis A A, Abanin D A, Serbyn M and Papić Z 2018 Weak ergodicity breaking from quantum many-body scars *Nat. Phys.* **14** 745
- [11] Turner C J, Michailidis A A, Abanin D A, Serbyn M and Papić Z 2018 Quantum scarred eigenstates in a Rydberg atom chain: Entanglement, breakdown of thermalization, and stability to perturbations *Phys. Rev. B* **98** 155134
- [12] Shiraishi N 2019 Connection between quantum-many-body scars and the Affleck-Kennedy-Lieb-Tasaki model from the viewpoint of embedded Hamiltonians *J. Stat. Mech.* 083103
- [13] Lin C-J and Motrunich O I 2019 Exact Quantum Many-Body Scar States in the Rydberg-Blockaded Atom Chain *Phys. Rev. Lett.* **122** 173401
- [14] Choi S, Turner C J, Pichler H, Ho W W, Michailidis A A, Papić Z, Serbyn M, Lukin M D and Abanin D A 2019 Emergent SU(2) Dynamics and Perfect Quantum Many-Body Scars *Phys. Rev. Lett.* **122** 220603
- [15] Khemani V, Hermele M and Nandkishore R 2020 Localization from Hilbert space shattering: From theory to physical realizations *Phys. Rev. B* **101** 174204
- [16] Dooley S and Kells G 2020 Enhancing the effect of quantum many body scars on dynamics by minimizing the effective dimension *Phys. Rev. B* **102** 195114
- [17] Dooley S 2021 Robust Quantum Sensing in Strongly Interacting Systems with Many-Body Scars *PRX Quantum* **2** 020330
- [18] Schechter M and Iadecola T 2019 Weak Ergodicity Breaking and Quantum Many-Body Scars in Spin-1 XY Magnets *Phys. Rev. Lett.* **123** 147201
- [19] Iversen M and Nielsen A E B 2023 Tower of quantum scars in a partially many-body localized system *Phys. Rev. B* **107** 205140
- [20] Zhang J, Pagano G, Hess P W, Kyprianidis A, Becker P, Kaplan H, Gorshkov A V, Gong Z X and Monroe C 2017 Observation of a Many-Body Dynamical Phase Transition with a 53-Qubit Quantum Simulator *Nature (London)* **551** 601
- [21] Bernien H, Schwartz S, Keesling A, Levine H, Omran A, Pichler H, Choi S, Zibrov A S, Endres M, Greiner M, Vuletić V and Lukin M D 2017 Probing Many-Body Dynamics on a 51-Atom Quantum Simulator *Nature (London)* **551** 579
- [22] Barends R, Lamata L, Kelly J, García-Álvarez L, Fowler A G, Megrant A, Jeffrey E, White T C, Sank D, Mutus J Y, Campbell B, Chen Y, Chen Z, Chiaro B, Dunsworth A, Hoi I-C, Neill C, O'Malley P J J, Quintana C, Roushan P, Vainsencher A, Wenner J, Solano E and Martinis J M 2015 Digital Quantum Simulation of Fermionic Models with a Superconducting Circuit *Nat. Commun.* **6** 7654
- [23] Davis E J, Periwal A, Cooper E S, Bentsen G, Evered S J, Van Kirk K and Schleier-Smith M H 2020 Protecting Spin Coherence in a Tunable Heisenberg Model *Phys. Rev. Lett.* **125** 060402

- [24] Signoles A, Franz T, Ferracini Alves R, Gärttner M, Whitlock S, Zürn G and Weidemüller M 2021 Glassy Dynamics in a Disordered Heisenberg Quantum Spin System *Phys. Rev. X* **11** 011011
- [25] Trotzky S, Cheinet P, Fölling S, Feld M, Schnorrberger U, Rey A M, Polkovnikov A, Demler E A, Lukin M D and Bloch I 2008 Time-Resolved Observation and Control of Superexchange Interactions with Ultracold Atoms in Optical Lattices *Science* **319** 295
- [26] Gross C and Bloch I 2017 Quantum Simulations with Ultracold Atoms in Optical Lattices *Science* **357** 995
- [27] Keselman A, Balents L and Starykh O A 2020 Dynamical Signatures of Quasiparticle Interactions in Quantum Spin Chains *Phys. Rev. Lett.* **125** 187201
- [28] Bera A K, Wu J, Yang W, Bewley R, Boehm M, Xu J, Bartkowiak M, Prokhnenko O, Klemke B, Islam A T M N, Law J M, Wang Z and Lake B 2020 Dispersions of many-body Bethe strings *Nat. Phys.* **16** 625
- [29] Chauhan P, Mahmood F, Changlani H J, Koohpayeh S M and Armitage N P 2020 Tunable Magnon Interactions in a Ferromagnetic Spin-1 Chain *Phys. Rev. Lett.* **124** 037203
- [30] Babenko C, Göhmann F, Kozłowski K K, Sirker J and Suzuki J 2021 Exact Real-Time Longitudinal Correlation Functions of the Massive XXZ Chain *Phys. Rev. Lett.* **126** 210602
- [31] Fukuhara T, Schauß P, Endres M, Hild S, Cheneau M, Bloch I and Gross C 2013 Microscopic observation of magnon bound states and their dynamics *Nature (London)* **502** 76
- [32] Jepsen P N, Amato-Grill J, Dimitrova I, Ho W W, Demler E and Ketterle W 2020 Spin transport in a tunable Heisenberg model realized with ultracold atoms *Nature (London)* **588** 403
- [33] Popkov V and Presilla C 2016 Obtaining pure steady states in nonequilibrium quantum systems with strong dissipative couplings *Phys. Rev. A* **93** 022111
- [34] Popkov V and Schütz G M 2017 Solution of the Lindblad equation for spin helix states *Phys. Rev. E* **95** 042128
- [35] Popkov V, Prosen T and Zadnik L 2020 Exact Nonequilibrium Steady State of Open XXZ/XYZ Spin-1/2 Chain with Dirichlet Boundary Conditions *Phys. Rev. Lett.* **124** 160403
- [36] Popkov V, Zhang X and Klümper A 2021 Phantom Bethe Excitations and Spin Helix Eigenstates in Integrable Periodic and Open Spin Chains *Phys. Rev. B* **104** L081410
- [37] Jepsen P N, Ho W W, Amato-Grill J, Dimitrova I, Demler E and Ketterle W 2021 Transverse Spin Dynamics in the Anisotropic Heisenberg Model Realized with Ultracold Atoms *Phys. Rev. X* **11** 041054
- [38] Hild S, Fukuhara T, Schauß P, Zeiher J, Knap M, Demler E, Bloch I and Gross C 2014 Far-from-Equilibrium Spin Transport in Heisenberg Quantum Magnets *Phys. Rev. Lett.* **113** 147205
- [39] Jepsen P N, Lee Y K, Lin H Z, Dimitrova I, Margalit Y, Ho W W and Ketterle W 2022 Long-lived phantom helix states in Heisenberg quantum magnets *Nat. Phys.* **18** 899
- [40] Stagraczyński S, Chotorlishvili L, Schüler M, Mierzejewski M and Berakdar J 2017 Many-body localization phase in a spin-driven chiral multiferroic chain *Phys. Rev. B* **96** 054440
- [41] Mark D K, Lin C-J and Motrunich O I 2020 Unified structure for exact towers of scar states in the Affleck-Kennedy-Lieb-Tasaki and other models *Phys. Rev. B* **101** 195131
- [42] Kuno Y, Mizoguchi T and Hatsugai Y 2020 Flat band quantum scar *Phys. Rev. B* **102** 241115(R)
- [43] Moudgalya S, Regnault N and Bernevig B A 2020 η -pairing in Hubbard models: From spectrum generating algebras to quantum many-body scars *Phys. Rev. B* **102**, 085140
- [44] Zhang G and Song Z 2023 Quantum scars in spin-1/2 isotropic Heisenberg clusters *New J. Phys.* **25** 053025
- [45] Shi Y B and Song Z 2023 Robust unidirectional phantom helix states in the XXZ Heisenberg model with Dzyaloshinskii-Moriya interaction *Phys. Rev. B* **108** 085108
- [46] Ma E S, Zhang K L and Song Z 2022 Steady helix states in a resonant XXZ Heisenberg model with Dzyaloshinskii-Moriya interaction *Phys. Rev. B* **106** 245122
- [47] Oganesyan V and Huse D A 2007 Localization of interacting fermions at high temperature, *Phys. Rev. B* **75** 155111
- [48] Atas Y Y, Bogomolny E, Giraud O and Roux G 2013 Distribution of the Ratio of Consecutive

- Level Spacings in Random Matrix Ensembles *Phys. Rev. Lett.* **110** 084101
- [49] Laumann C R, Pal A and Scardicchio A 2014 Many-Body Mobility Edge in a Mean-Field Quantum Spin Glass *Phys. Rev. Lett.* **113** 200405
- [50] Dong H, Desaulles J Y, Gao Y, Wang N, Guo Z X, Chen J C, Zou Y R, Jin F T, Zhu X H, Zhang P F, Li H K, Wang Z, Guo Q J, Zhang J X, Ying L and Papić Z 2023 Disorder-tunable entanglement at infinite temperature *Sci Adv.* **9** 51
- [51] Mikeska H-J and Kolezhuk A 2004 One-dimensional magnetism *Lect. Notes Phys.* **645** 1
- [52] Anderson P W 1967 Infrared Catastrophe in Fermi Gases with Local Scattering Potentials *Phys. Rev. Lett.* **18** 1049
- [53] Anderson P W 1967 Ground State of a Magnetic Impurity in a Metal *Phys. Rev.* **164** 352